Int. J. Electrochem. Sci., 12 **(2017)** 10129 – 10139, doi: 10.20964/2017.11.22

International Journal of
ELECTROCHEMICAL
SCIENCE
www.electrochemsci.org

Detection of Calcitonin in Medullary Thyroid Carcinoma by an Electrochemical Sensor

Deshun sha[1], *Baozhong Zhuge*[2,*] *and Feng Lin*[3]

[1] Department of Laboratory Medicine, The people's hospital of guan, Liaocheng City, Shandong Province, 276003, P.R. China
[2] Department of Laboratory Medicine, Linyi People's Hospital, No.27, East Jiefang road, Linyi City, Shandong Province, 276003, P.R. China
[3] Department of Oncology, The Eighth People's Hospital of Shanghai, No.8, Caobao Road, Xu Hui District, Shanghai 200233, P.R. China
[*]E-mail: fenglin_linda@qq.com

Received: 8 July 2017 / *Accepted:* 2 September 2017 / *Published:* 12 October 2017

In this report, calcitonin (CT) was sensitively and selectively detected using a novel route in which a CT-imprinted polymer was synthesized on the surface of TiO_2 NPs using a surface molecular imprinting strategy. The sensor derived from the above polymer was capable of detecting slight variations in the human body CT concentration. For clinical analysis, this kind of sensor has potential to provide a reliable, disposable, renewable and cost-effective approach that avoids the matrix effect and cross-reactivity from real specimens.

Keywords: Thyroid medullary carcinoma; Electrochemical immunoassay; TiO_2; Molecular imprinting; Calcitonin

1. INTRODUCTION

Medullary thyroid carcinomas (MTCs), generated from the parafollicular cells of the thyroid that secrete calcitonin (CT), are rare, representing 4–10% of all malignant thyroid neoplasms [1]. Approximately 25% of MTCs are familial forms that can be detected through molecular screening for mutations in the rearranged during transfection protooncogene [2], while most forms are sporadic [3]. Due to the frequent involvement of lymph nodes or distant metastases at the point of diagnosis (even in the case of a rather small primary tumor), an undesirable prognosis is always seen [4-7]. To improve the MTC-related morbidity and mortality, early diagnosis and radical surgical treatment are of vital significance.

Based on reported results, both MTC and C cell hyperplasia (CCH) (a preneoplastic lesion in the familial forms of MTC [8]) can be detected at an earlier stage through the routine measurement of the serum CT level in patients with thyroid nodules. However, there is no evidence that the sporadic forms of CCH undergo a malignant transformation. Although this sort of screening has been evaluated in several studies [9-12], controversy still exists [13-16]. Additionally, considering the current problem of the cost-effectiveness of the method, the American Thyroid Association has not proposed a recommendation in terms of this practice. According to this association, confirmatory testing after stimulation with pentagastrin (PG), which is not available in the USA markets, could enhance the specificity of CT screening in a majority of measurements [17]. However, the European Thyroid Association recently reported a recommendation for serum CT measurement in the initial diagnostic assessment of thyroid nodules [18] without providing suggestions in terms of the measurement routes, result interpretation, and application of stimulation testing.

CT determination can be applied to the biomarking of medullary thyroid carcinoma (MTC), osteoporosis and malignant tumors [19]. Based on the table reported by Costante and co-workers in January 2009, the normal range of CT in the body is below 10 ng/L. C-cell hyperplasia may occur at a concentration range of 100 and 500 ng/L, and medullary thyroid carcinoma (MTC) is possible at a concentration above 500 ng/L. In addition, the established presence of MTC in the body was suggested to have a concentration of over 1000 ng/L [20]. Several approaches to CT determination have been reported, including radioimmunoassay [21], enzyme-linked immunosorbent assay [22], high-performance liquid chromatography (HPLC) [23], time-resolved fluoroimmunoassay [24], two-site immunofluorometric assay [25] and room temperature phosphorescence immunoassay [26]. However, the above routes suffer certain drawbacks, such as the harm of the radioactive contamination in the radioimmunoassay to human health. In addition, other immunoassay strategies involve time-consuming determination processes or complex manipulation. Hence, it remains necessary to develop a facile, sensitive and cost-effective route to the clinical determination of CT.

Since electrochemical strategies are highly simple, sensitive, time-saving, and cost-effective, they have gained extensive attention in the field of sensitive detection of cancer markers in biological fluids, although these strategies are less selective [27]. Molecular recognition elements could be used in electrochemical strategies to improve the poor selectivity, and among these elements, molecularly imprinted polymers (MIPs) is one of the most common methods applied to electrochemical strategies based on previous reports [28, 29]. MIPs consist of a polymer network generated from monomer molecules with a cross-linker around a target molecule, and after the extraction of the target molecule, a cavity is left that is specific to the shape and size of the template molecule. Small molecule-oriented MIPs are common and can be easily synthesized. Considering the solubility factor, size, and structural complexity, the imprinting of large molecules such as proteins and other biomolecules remains difficult [30]. The water-soluble property of most proteins constitute a main problem during the fabrication of an MIP in organic solvent, leading to a decreased binding capacity and site accessibility in the 3D polymer matrix [31]. Different techniques have been reported for the successful imprinting of proteins to solve the above problems, including surface imprinting [32], an epitope approach [33] and the use of low cross-linking density hydrogels [34]. Generally, the imprinted sites are placed on the material surface or adjacent to the surface through surface imprinting. The entrapment of a protein

template can be limited in cross-linked polymers. Surface imprinting of nanosized spheres can not only be used as a proper template of proteins and other bulky structures but can also support materials with large specific surface areas. On the other hand, nanostructured materials possess distinct and varying magnetic, mechanical, optical, and electrical features and provide a higher ratio of surface to volume than micro-sized particles [35].

In this work, a CT-imprinted polymer was prepared using TiO_2 as a platform. This was followed by coating the monomer-decorated TiO_2, cross-linker, reducing agent, catalyst, initiator, and template on a vinyl group-decorated pencil graphite electrode (PGE). In either blood specimens or aqueous media, our developed sensor was highly selective and sensitive to the detection of CT molecules. Furthermore, the as-prepared sensor is applicable to the low-cost and rapid diagnosis of bone cancer through the accurate monitoring of CT concentration.

2. EXPERIMENTS

2.1. Chemicals

Human CT, thionyl chloride, L-tyrosine, ascorbic acid, copper(II) chloride ($CuCl_2$), 2,2′-bipyridyl, triethoxy vinyl silane, ethylene glycol dimethacrylate, titanium butoxide, and other interference agents, including globulin, albumin, citric acid, insulin, proinsulin C-peptide, porcine CT, and salmon CT, were commercially available from Sigma-Aldrich. All other reagents were of analytical grade and used without additional purification. A mixture of K_2HPO_4 and KH_2PO_4 (0.1 M) was adjusted to the proper pH and used as phosphate buffer solution (PBS). Milli-Q water (18.2 MΩ cm) was used throughout the experiments.

2.2. Instruments

A CHI 660C workstation equipped with a triple-electrode geometry was used for all electrochemical determinations, with MIP-decorated PGE as the working electrode, Ag/AgCl (3.0 M KCl) as the reference electrode, and a platinum wire as the counter electrode. Fourier transform infrared spectrometers from Varian were used to perform the IR experiments to characterize the binding. A Quanta chrome Nova 3200e surface area and pore size analyzer was used for the nitrogen adsorption investigation. All measurements were performed at ambient temperature (25 ± 1 °C). CuKα radiation was applied to a Bruker D8 Advance instrument for the powder X-ray diffraction (XRD) investigation.

2.3. Synthesis of the TiO_2-modified 2-acryloylamino-3-(4-hydroxy-phenyl)-propionic acid monomer

A simple hydrothermal route proposed by Lui and co-workers [36] with minimal modification was used for the preparation of TiO_2 NPs. A mixture of acetic acid (20 mL) and titanium butoxide (2 mL) was stirred for 30 min before being delivered to a Teflon-lined stainless-steel autoclave (50 mL), heated to 150 °C in an oven for 10 h, and natural cooled to ambient temperature. Afterwards, the

mixture was centrifuged, with the sediment collected and washed. Finally, TiO_2 NPs were obtained after heating to 500°C.

The monomer was synthesized by dissolving 3.62 g of 4-hydroxy-phenyl-propionic acid into aqueous NaOH (1 M, 10 mL) under 10 min stirring, which was cooled in ice water. This dissolution step was followed by slow addition of acryloyl chloride (0.5 M, 0.8 mL) under 60 min of stirring at 40 °C. The pH was kept at 2.0 throughout. The compound obtained after the reaction was terminated was extracted using ethyl acetate and dried to give a yield of 87%.

The surface of TiO_2 was functionalized by covalently attaching the obtained monomer. Specifically, a dispersion of distilled water (20 mL) and 0.1 g of TiO_2 was introduced into a mixture of water (10 mL) and 0.1 g of 2-acryloylamino-3-(4-hydroxy-phenyl)-propionic acid monomer and refluxed for 60 min at 60–70 °C. The solution pH was kept at 4 to 5 throughout the reaction. The final product obtained after the reaction was washed using water and dried at ambient temperature.

2.4. Fabrication of the calcitonin-imprinted TiO_2-modified PGE

The electrode was prepared after the pretreatment of pencil graphite lead with nitric acid (6.0 M) for 15 min and washing with water. This pretreatment step was followed by cleaning the surface of the lead by it rubbing with cotton and drying at ambient temperature. The PGE was prepared by housing the 5-mm-long pencil lead (diameter, 0.5 mm) in a micropipette tip. In addition, a metallic wire was wrapped around one end of the lead, with the other end free for additional modification, to achieve electrical contact. The modification of the electrode began with the generation of double bonds on the PGE surface along with the synthesis of the MIP, followed by decoration of the electrode with hydrolyzed vinyl silane. Silane was hydrolyzed by mixing triethoxy vinyl silane (1 mL) with ethanol (1 mL) and water (0.5 mL) and then adding 2–3 drops of HCl under 30 min of stirring. This was followed by dipping the as-prepared electrode in a specimen vial that contained the hydrolyzed vinyl silane for 10 to 15 min and drying at ambient temperature.

2.5. Electrochemical determination

An electrochemical cell was used throughout the voltammetric investigations. Prior to measurement, the accumulation of analyte was performed under the following optimal parameters: accumulation time, 1 min; accumulation potential, −0.5 V (*vs.* Ag/AgCl), and 15 s equilibration. Afterwards, DPSV profiles were plotted using the following the parameters: scan rate, 0.01 V/s; pulse width, 50 ms; pulse amplitude, 25 mV; and potential range, −0.3 V to −1.2 V (*vs.* Ag/AgCl). We also recorded the CVs within the potential window range of +1.5 to −2.0 V (*vs.* Ag/AgCl) with varying the scan rate.

3. RESULTS AND DISCUSSION

The obtained TiO_2 nanostructures were characterized via the XRD profiles shown in Fig. 1A. Broad peaks at 68.88°, 67.89°, 66.32°, 62.77°, 56.56°, 47.53°, 36.21°, 34.48°, and 31.61° were

observed, and these peaks were consistent with those of the standard JCPDS file for TiO_2. For the measurement of the UV–vis absorption spectrum, the specimen was dispersed in double-distilled water as a reference. As shown in the UV–vis spectrum in Fig. 1B, an insignificant but discernable peak was observed in the UV domain due to the excitonic absorption peak of ZnO.

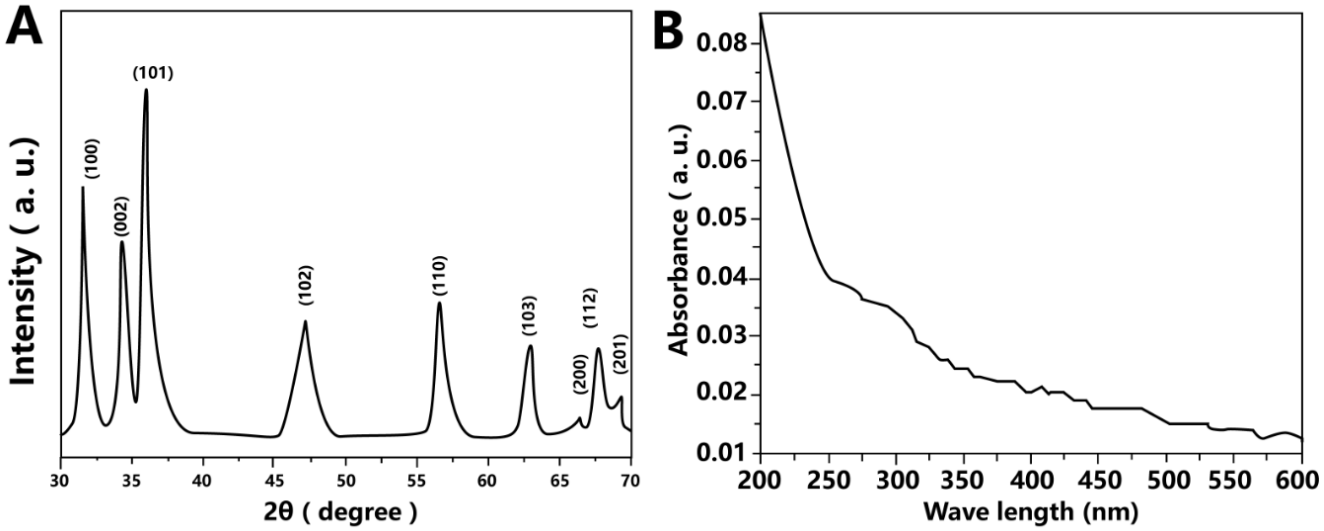

Figure 1. (A) XRD pattern and (B) UV–vis spectrum of the TiO_2 NPs.

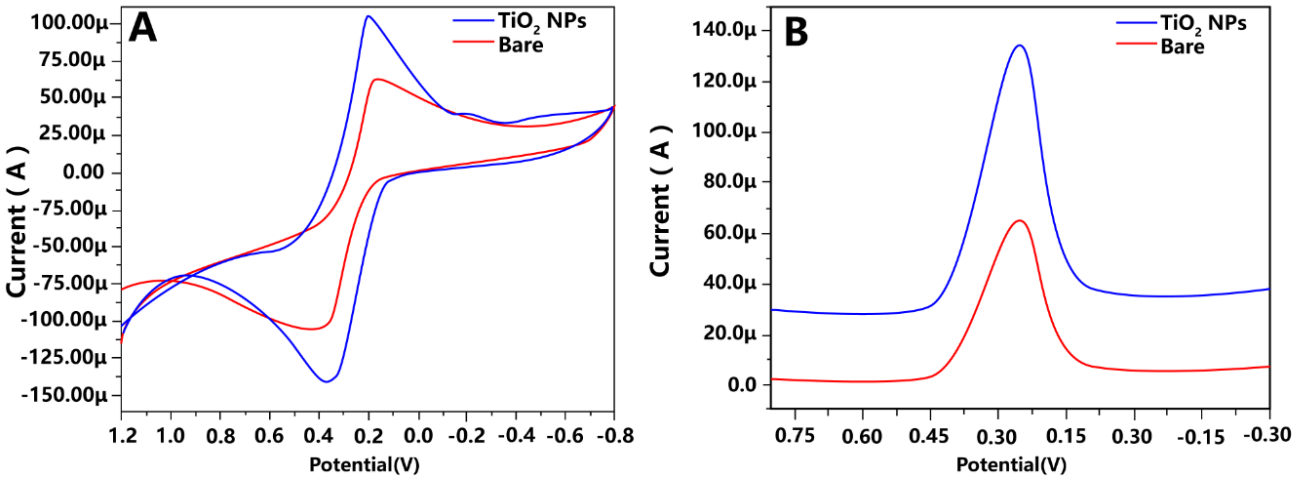

Figure 2. (A) CV and (B) differential pulse stripping voltammetric (DPSV) measurement of the original and TiO_2 NP-decorated PGE using $K_3Fe(CN)_6$ (5.0 mM).

The electrocatalytic performance of the TiO_2 NPs was investigated in a pH 8.0 KCl solution that contained $K_3Fe(CN)_6$ (5.0 mM) as an electrochemical probe. An oxidation peak and a reduction peak were observed at +0.35 V and +0.18 V, respectively, in the cyclic voltammogram (CV) of $K_3Fe(CN)_6$ using the original PGE (Fig. 2A). Upon the immobilization of TiO_2 NPs on the electrode, a fourfold increase in the peak current was observed, since the nanoparticles coating promoted an

increase in the effective working electrode surface area. As shown in Fig. 2B, the DPSV measurement provided similar results, confirming the enhancement of the electrocatalytic activity by the deposition of TiO_2 NPs on the PGE surface. This result confirms the dual behavior of the TiO_2 NPs of increasing the imprinting efficiency and the enhancing the electrochemical properties [37, 38].

A series of electrodes, including the original PGE, silica-decorated PGE, TiO_2 NP-decorated PGE, MIP-decorated PGE, and MIP/TiO_2 NP-decorated PGE, were used in electrochemical measurements to investigate the role of the TiO_2 NPs in the calcitonin estimation. Table 1 displays the corresponding results. Compared with the original PGE and the silica-modified PGE, the TiO_2 NP-decorated PGE exhibited a more desirable current response, indicating the corresponding electrochemical role. However, the MIP/TiO_2 NP-decorated PGE showed the highest current response, as shown in Fig. 3A. The kinetic and electrochemical factors of the calcitonin molecule were determined by carrying out CV investigations within the potential range of +1.5 to −2.0 V (scan rate 0.01–0.5 V/s). Fig. 3B shows that a single reduction peak at −0.6 Vs was observed when the scan rate was low, indicating that the calcitonin molecule reduction as irreversible. Nevertheless, an oxidation peak at +0.3 V was observed in the reverse scan when the scan rate was increased, which indicated that this process was quasi-reversible. According to the literature, the cathodic peak is attributed to the reduction of the disulfide bond present in the protein molecule to free thiol groups [39]. At a low scan rate, the —S—S— bond is reduced to a free thiol group and the 3D structure of the protein is destroyed, but at a higher scan rate, there is not enough time for the structural degradation of the protein molecule, and the reaction can then be reversed upon scanning in the opposite direction [40].

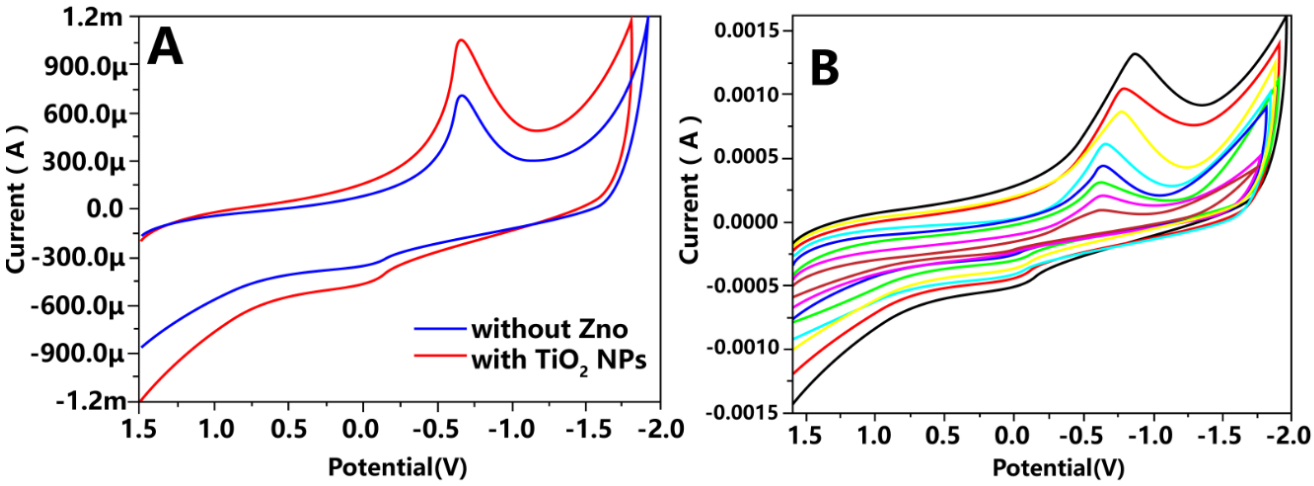

Figure 3. (A) CV scans of the PGEs decorated with imprinted polymer (before and after adding TiO_2 NPs). (B) CV scans collected at a scan rate of 0.01 - 0.5 V/s.

For the chronocoulometry (CC) investigation, the charge was plotted *vs.* the time response to an applied potential step waveform. The *Q–t* curves obtained for the blank background solution and calcitonin using the NIP-coated PGE, the original PGE, and the MIP-decorated PGE are compared in Fig. 4A. For the blank solution, the CC response could be neglected since the charge is the integration of the current. The MIP-decorated electrode exhibited the highest CC response to calcitonin. The

number of cavities on the surface of the electrode was determined to be 1.72×10^{16} for the case of a single template molecule binding to one MIP cavity.

Table 1. Comparative study of a series of decorated electrodes and the original electrode in the detection of calcitonin.

Name of electrode	Current in CV (mA)	Current in DPSV (μA)
Bare PGE	0.14	10.13
Silica coated PGE	0.12	8.22
TiO_2 NPs coated PGE	0.18	15.05
Imprinted PGE without TiO_2 NPs	0.63	13.14
Imprinted PGE with TiO_2 NPs	1.08	34.47

Electrochemical impedance spectroscopy (EIS) is a powerful tool for studying the interfacial properties of surface-modified electrodes and the electron transfer resistance at the electrode surface [41-43]. The semicircle diameter in the impedance spectrum (presented in the form of a Nyquist plot) equals the charge transfer resistance, Rct, which is related to the charge transfer kinetics of the redox probe on the electrode surface. The electrochemical impedance spectra of the original PGE, the MIP-decorated PGE, the MIP-decorated PGE with calcitonin rebound and the non-imprinted polymer (NIP)-decorated PGE are shown in Fig. 4B. The original PGE showed a charge transfer resistance (R_{ct}) of 4.6 kΩ, which is comparable to that of the imprinted sensor (4.9 kΩ). Nevertheless, after 60.0 μg L^{-1} of the template molecule was bound, an increase in the resistance was observed. It can be seen that the MIP-decorated PGE and the MIP-decorated PGE after template rebinding showed different R_{ct} values, which was due to the selective rebinding of the template on the MIP membrane, further leading to blockage of the available cavities as well as a lowered charge transfer, viz., a higher R_{ct} value. On the other hand, the resistance of the non-imprinted sensor was found to be much higher. This high resistance indicates that the polymer membrane does not have available recognition sites and is probably not a good conductive surface for electrochemical processes [44, 45].

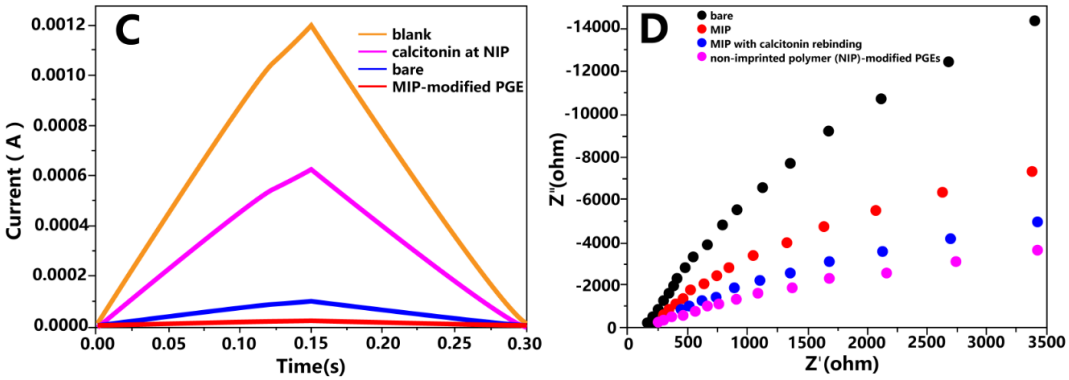

Figure 4. (A) Chronocoulometry scans (*Q–t* curves) before and after addition of calcitonin to the solution using the NIP-coated PGE, the original PGE and the MIP-decorated PGE. (D) Nyquist diagrams of CT using the original PGE, the MIP-decorated PGE, the MIP-decorated PEG with CT rebound and the non-imprinted polymer (NIP)-decorated PGE.

The pH of the supporting electrolyte was optimized by placing the MIP-decorated electrode into an electrochemical cell that contained 60.0 μg/L CT, and 10 mL phosphate buffer with different pH values (2.0 to 12.0) and recording the DPSV measurement. As the pH increased, an increase in the DPSV current was observed, which then reached its maximal value when the pH was 12. Compared with the traditional CV measurements, DPSV was more sensitive towards the quantitative detection of CT. The DPSV measurements of CT at varying concentrations are shown in Fig. 5. As the CT concentration increased, an increase in the peak current was observed, indicating the increased number of binding sites in the film that were occupied by the template molecule. For the calibration curve, the concentration of CT (10 ng/L to 900 μg/L) using the MIP electrode under the optimum conditions was found to be linearly related to the DPSV peak current for the reduction of CT. After three repeated analyses, the limit of detection (LOD) was calculated to be as low as 3.5 ng/L, which suggested that our developed sensor was highly sensitive.

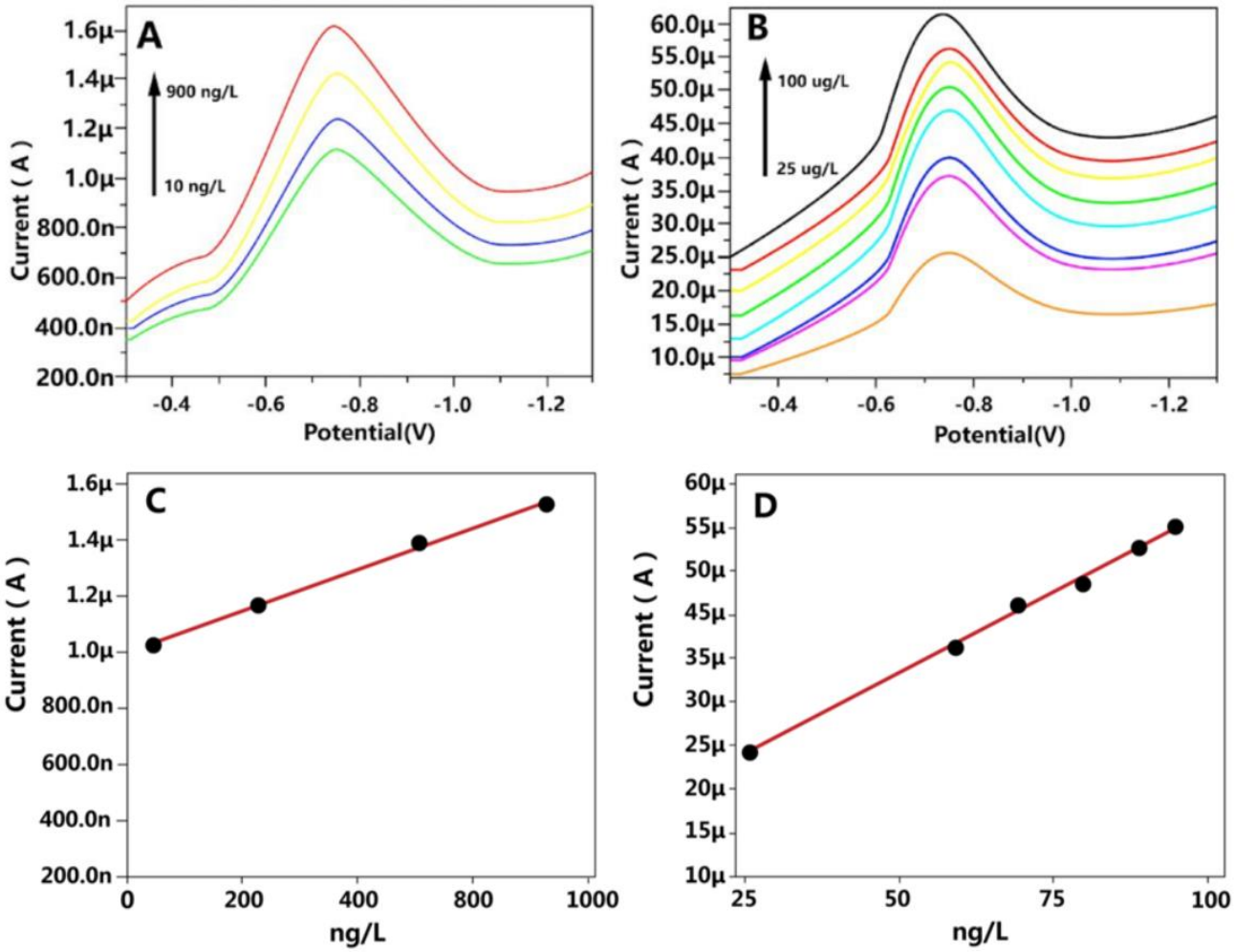

Figure 5. (A) DPSV response to CT using the MIP-decorated PGE with increasing CT concentration from 0 to 900 ng/L. (B) DPSV response to CT from 25 to 100 μg/L with an accumulation time of 60 s and an accumulation potential of −0.5 V in a phosphate buffer solution (pH 12). (C, D) Calibration curves of the concentrations against the currents in (A, B).

Table 2 shows the comparison in the detection of CT using our developed route and other previously reported routes. In this comparison, our proposed route showed a lower LOD and a more desirable dynamic linear range. We also compared the detection of CT by the as-prepared sensor and the commercially available ELISA kit.

Table 2. Comparison of the proposed work with some other reported commercial and research methods for CT determination.

Method	Linear Range	LOD	Ref
ELISA kit	12.35-1000 ng/L	4.58 ng/L	Product
Biovendor ELISA kit	10–400 ng/L	0.7 ng/L	Product
Alpco ELISA kit	10-1000 ng/L	1.0 ng/L	[39]
HPLC with electrochemical	0.5-20 ng	0.1 ng	[46]
SSRTPIA	0.04-4.0 fg/spot	2 ng L^{-1}	[26]
HPLC	3-30 mg/L	0.5 mg L^{-1}	[47]
IMFM assay	0.3-300 pM	0.15 pM	[25]
Proposed sensor	10 ng/L-8mg/L	3.5 ng/L	This work

4. CONCLUSIONS

To detect an ultra-trace-level biomarker, an electrochemical sensor was prepared based on a new medullary thyroid carcinoma marker-imprinted polymer that was synthesized on the surface of TiO_2 NPs. CT at trace levels was successfully detected using the polymer molecularly imprinted with the CT molecule. This report also investigated the electrochemical performance of a sensor derived from the polymer in the detection of the CT molecule. Our proposed sensor was highly reproducible and had a desirable LOD, confirming that this sensor could be successfully applied to CT determination in real samples.

References

1. A.Giraudet, D. Vanel, S. Leboulleux, A. Aupérin, C. Dromain, L. Chami, N. Ny Tovo, J. Lumbroso, N. Lassau and G. Bonniaud, *The Journal of Clinical Endocrinology & Metabolism*, 92 (2007) 4185.
2. S. Ong, H. Schöder, S. Patel, I. Tabangay-Lim, I. Doddamane, M. Gönen, A. Shaha, R. Tuttle, J.P. Shah and S. Larson, *Journal of Nuclear Medicine*, 48 (2007) 501.
3. M. Bugalho, J. Santos and L. Sobrinho, *Journal of Surgical Oncology*, 91 (2005) 56.
4. H. Vierhapper, B. Niederle, C. Bieglmayer, K. Kaserer and S. Baumgartner-Parzer, *Thyroid*, 15 (2005) 1267.
5. A. Giraudet, A. Al Ghulzan, A. Aupérin, S. Leboulleux, A. Chehboun, F. Troalen, C. Dromain, J. Lumbroso, E. Baudin and M. Schlumberger, *European Journal of Endocrinology*, 158 (2008) 239.
6. M. Iacobone, P. Niccoli-Sire, F. Sebag, C. De Micco and J. Henry, *World Journal of Surgery*, 26 (2002) 886.
7. A. Redding, S. Levine and M. Fowler, *Thyroid*, 10 (2000) 919.
8. J. Meijer, S. Le Cessie, W.B. Van Den Hout, J. Kievit, J. Schoones, J. Romijn and J.. Smit, *Clinical*

Endocrinology, 72 (2010) 534.
9. B. Herrmann, K. Schmid, R. Goerges, M. Kemen and K. Mann, *European Journal of Endocrinology*, 162 (2010) 1141.
10. K. Tran, S. Khan, M. Taghizadehasl, F. Palazzo, A. Frilling, J. Todd and A. Al-Nahhas, *Hellenic Journal of Nuclear Medicine*, 18 (2015) 19.
11. L. Giovanella, F.A. Verburg, M. Imperiali, S. Valabrega, P. Trimboli and L. Ceriani, *Clinical Chemistry and Laboratory Medicine*, 51 (2013) 1477.
12. K. Lorenz, M. Elwerr, A. Machens, M. Abuazab, H. Holzhausen and H. Dralle, *Langenbeck's Archives of Surgery*, 398 (2013) 403.
13. S. Patra, E. Roy, R. Madhuri and P. Sharma, *Anal. Chim. Acta.*, 853 (2015) 271.
14. H. Kwon, W. Kim, Y. Choi, E. Jang, M. Jeon, D. Song, J. Baek, J. Ryu, S. Hong and T.Y. Kim, *Clinical Endocrinology*, 82 (2015) 598.
15. P. Rosário, G. Penna, K. Brandão and B. Souza, *Arquivos Brasileiros de Endocrinologia & Metabologia*, 57 (2013) 312.
16. P. Trimboli, L. Guidobaldi, M. Bongiovanni, A. Crescenzi, M. Alevizaki and L. Giovanella, *Diagnostic Cytopathology*, 44 (2016) 45.
17. C. De Crea, M. Raffaelli, D. Maccora, C. Carrozza, G. Canu, G. Fadda, R. Bellantone and C. Lombardi, *Acta Otorhinolaryngologica Italica*, 34 (2014) 399.
18. T. Koopman, C. Niedlich-den Herder, C. Stegeman, T. Links, J. Bijzet, B. Hazenberg and A. Diepstra, *American Journal of Kidney Diseases*, 69 (2017) 546.
19. G. Costante, C. Durante, Z. Francis, M. Schlumberger and S. Filetti, *Nature Clinical Practice Endocrinology & Metabolism*, 5 (2009) 35.
20. R. Batista, A. Toscanini, L. Brandão and M. Cunha-Neto, *Indian Journal of Endocrinology and Metabolism*, 17 (2013) 524.
21. E. Cavalier, A. Carlisi, J. Chapelle and P. Delanaye, *Clinical Chemistry*, 54 (2008) 929.
22. C. Lynch, R. Seth, D. Bates and C. Self, *Journal of Immunoassay and Immunochemistry*, 9 (1988) 179.
23. R. Buck and F. Maxl, *Journal of Pharmaceutical and Biomedical Analysis*, 8 (1990) 761.
24. H. Rong, O. Tørring, M. Sääf, U. Sjöstedt, H. Sjöberg and E. Bucht, *Clinical Chemistry*, 40 (1994) 1774.
25. L. Deftos, *Clinical Chemistry*, 38 (1992) 2284.
26. J. Liu, X. Huang, L. Zhang, Z. Zheng, X. Lin, X. Zhang, L. Jiao, M. Cui, S. Jiang and S. Lin, *Anal. Chim. Acta*, 744 (2012) 60.
27. M. Tabeshnia, H. Heli, A. Jabbari and A. Moosavi-Movahedi, *Turk. J. Chem.*, 34 (2010) 35.
28. G. Vasapollo, R. Sole, L. Mergola, M. Lazzoi, A. Scardino, S. Scorrano and G. Mele, *International Journal of Molecular Sciences*, 12 (2011) 5908.
29. A. Tiwari, S. Deshpande, H. Kobayashi and A. Turner, *Biosensors and Bioelectronics*, 35 (2012) 224.
30. S. Li, A. Tiwari, Y. Ge and D. Fei, *Adv. Mater. Lett*, 1 (2010) 4.
31. R. Ouyang, J. Lei and H. Ju, *Chemical Communications*, (2008) 5761.
32. H. Shi, W. Tsai, M. Garrison, S. Ferrari and B. Ratner, *Nature*, 398 (1999) 593.
33. H. Nishino, C. Huang and K. Shea, *Angewandte Chemie International Edition*, 45 (2006) 2392.
34. D. Tong, C. Heényi, Z. Bikadi, J.P. Gao and S. Hjerten, *Chroma*, 54 (2001) 7.
35. Y. Yin and A. Alivisatos, *Nature*, 437 (2005) 664.
36. X. Liu, X. Li, Y. Xiong, Q. Huang, X. Li, Y. Dong, P. Liu and C. Zhang, *Microchim. Acta*, 180 (2013) 1309.
37. H. Moghaddam, H. Beitollahi, S. Tajik, I. Sheikhshoaie and P. Biparva, *Environmental Monitoring and Assessment*, 187 (2015) 407.
38. A. Hayat, A. Rhouati, R. Mishra, G. Alonso, M. Nasir, G. Istamboulie and J. Marty, *International Journal of Environmental Analytical Chemistry*, 96 (2016) 237.

39. J. Osteryoung and K. Wikiel, *Analytica Chimica Acta*, 351 (1997) 65.
40. J. Cui, J. Chen, S. Chen, L. Gao, P. Xu and H. Li, *Nanotechnology*, 27 (2016) 095603.
41. J. Carrera-Crespo, M. Rincón, F. González, E. Barrera and I. González, *Journal of Solid State Electrochemistry*, 20 (2016) 2713.
42. S. Kang, L. Zhang, C. Liu, L. Huang, H. Shi and L. Cui, *Int. J. Electrochem. Sci.*, 12 (2017) 5284.
43. F. Rahimi, J. Bebeau, O. Matar and A. Takshi, *Journal of Applied Electrochemistry*, 47 (2017) 305.
44. B. Rezaei, M. Taki and A. Ensafi, *Journal of Solid State Electrochemistry*, 21 (2017) 371.
45. J. Wei, J. Liu, Z. Wu, Z. Zhan, J. Shi and K. Xu, *Journal of Nanoscience and Nanotechnology*, 15 (2015) 5013.
46. H. Lee, S. Choi, H. Lee, C. Jeong, S. Kim, J. Lee, S. Yoo, P. DeLuca and K. Lee, *Chroma*, 50 (1999) 701.
47. X. Chen, Q. Guo and Q. Zhang, *Journal of Chinese Pharmaceutical Science*,12 (2003) 114